Magnetization of a type-I superconducting slab in the thermodynamic and the metastable phases

André Fortini, Alain Hairie, and Eric Paumier
Laboratoire de Physique du Solide de l'Université de Caen, 14 032 Caen Cedex, France*
(Received 19 June 1979)

The first magnetization law of an infinite slab of rectangular cross section, in a perpendicular applied field, is worked out along general ideas previously published. By neglecting penetration in the edges of the slab, assumed of small thickness, the complex potential is obtained in a simple way with the help of two successive Schwarz-Christoffel conformal mappings. The construction of the thermodynamic potential permits a detailed analysis of the ideal thermodynamic behavior which is, then, compared with the real one, based on a migration mechanism. Explicit calculations of the magnetic moment along with the thermodynamic and migration thresholds are carried out. The migration process is shown to give rise to a metastable phase, including a macroscopic current, and responsible for the currently observed hysteretic behavior.

I. INTRODUCTION

In Ref. 1 we have discussed the thermodynamics of the metastable process governing the magnetic-flux penetration into a nonellipsoidal type-I superconducting sample. The first stage of this process is concerned with the penetration in the edges up to the occurrence of the migration of domains into the bulk. A complete theoretical treatment of this stage, in the case of an infinite slab, placed in a perpendicular and uniform field, has been worked out in Ref. 2 by analytical and computational means, within the limits of a so-called macroscopic model.

The purpose of this paper is to work out a theoretical treatment of the second stage of magnetization in the slab, beyond the migration threshold. As discussed in Ref. 1 this stage is characterized by flux penetration both in the edges and the bulk. It is well confirmed by many observations on samples of different shapes.[3–9]

The analytical method used in Ref. 2 which is based on an appropriate extension of existing solutions of the Dirichlet's problem, could be extended to the present more complicated magnetic configuration, but it would lead to rather involved mathematics. For this reason we will restrict ourself, here, to the case of a thin slab which will permit a drastic simplification of the treatment. If the thickness l is much smaller than the length a of the cross section ($l \ll a$) the effect of the penetration in the edges on the magnetic behavior is known to be very small.[10–12] Ignoring this penetration, a mathematical description of the field distribution is possible by using elementary conformal mappings only. The price of this approximation is that the first-stage magnetization is reduced to a purely diamagnetic law, and some precision is lost in the determination of the migration threshold. On the other hand, the model will permit, in a quite simple and enlightened way, to bring out the metastable behavior of the penetration in the bulk, in which we are mainly interested.

We will also retain the macroscopic point of view of Ref. 2, in which the fine structure of the intermediate state is smoothed out into a continuous phase.

II. COMPLEX POTENTIAL FOR THE PENETRATION IN THE MEDIAN REGION OF THE SLAB

In Fig. 1 the half cross section of the slab (dimensions a,l) is represented in the xz plane with the configuration resulting from the penetration in the edges and in the bulk, which happens as the applied field H_0 is larger than the migration threshold H_m. Striped areas represent volumes in the intermediate state. It should be recalled that the internal equilibrium of these regions requires the magnetostatic field $\vec{H}$ to be of constant magnitude and the lines of force to be straight. This results in a fanlike configuration of the field and of the domain walls in the edges and, because of symmetry, in a uniform field with lines of force parallel to Oz, in the median region. The remarkable points of the configuration are noted $1, 2, 3, \ldots, \omega$, and symmetrically.

As in previous papers, we begin with the Schwarz-Christoffel transformation between the u plane and the ζ plane, defined by

$$\frac{du}{d\zeta} = -iB(\zeta^2 - k^2)^{1/2}(\zeta^2 - 1)^{-1/2} , \tag{1}$$

which transforms the contour $1234567\omega7'6'5'4'3'2'1'$ into the real axis $\xi'\xi$. By choosing the square-root real and positive when ζ is real and larger than 1, the

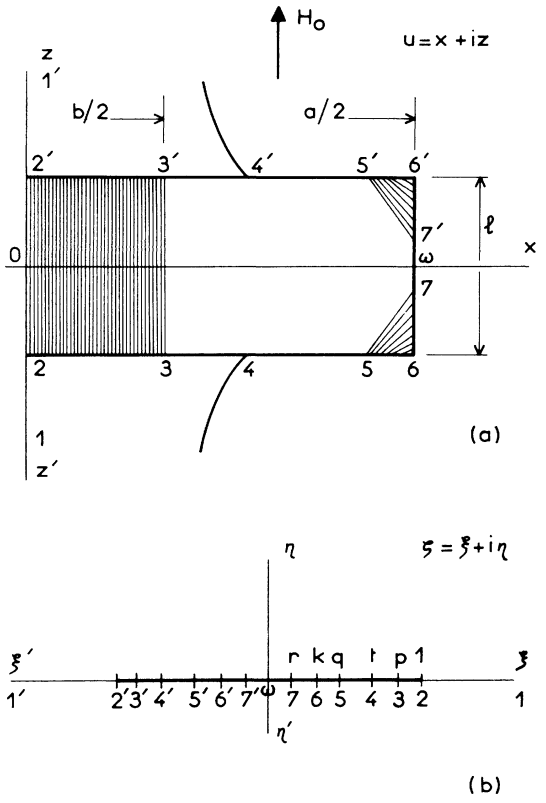

FIG. 1. Half cross section of the superconducting slab with flux penetration both in the edges and the median region, (a) in the $u(x,z)$ plane; (b) in the conformally transformed $\zeta(\xi,\eta)$ plane.

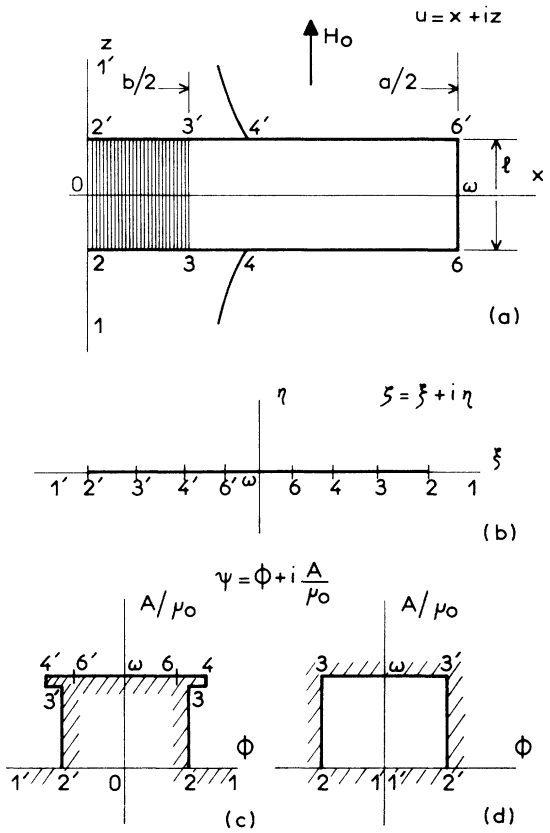

FIG. 2. Half cross section of the slab simplified by dropping penetration in the edges, (a) in the $u(x,z)$ plane; (b) in the $\zeta(\xi,\eta)$ plane; (c) and (d) in the $\psi(\phi,A/\mu_0)$ plane.

outside right part of the slab cross section corresponds to the upper half-plane $\eta \geq 0$. The abscissa of the points 2, 3, ..., are denoted by $\xi_2 = 1$, $\xi_3 = p$, ..., as indicated Fig. 1(b). The constants B, k, and p are related to the dimensions a, l of the slab and to the width b of the median region

$$B = a/2G_{k'} = l/2G_k = (la/4G_kG_{k'})^{1/2} \ , \tag{2}$$

$$b = 2BG_{k'}(\sin^{-1}p'/k') = aG_{k'}(\sin^{-1}p'/k')/G_{k'} \ , \tag{3}$$

where

$$G_k = E(\theta,k) - k'^2F(\theta,k) \ , \tag{4}$$

$k' = (1-k^2)^{1/2}$. $F(\theta,k)$, $E(\theta,k)$ denote, as usual, elliptic functions of the first, second kind, of modulus k and argument θ. If $\theta = \frac{1}{2}\pi$ the elliptic functions are said to be complete and the argument is dropped for brevity, $F(\frac{1}{2}\pi,k) = F_k$, etc.

The problem of seeking the complex potential of the external field distribution matched to the internal configuration of Fig. 1(a), is now reduced to a Dirichlet's problem for a half-plane with definite boundary conditions on the real axis and at infinity.

Within the above-mentioned simplification for the thin slab ($l \ll a$), the sketches of Fig. 1 are replaced with the ones of Figs. 2(a) and 2(b), in which 5,7 and 5′, 7′ are missing.

As in the previous papers, the field distribution will be represented by an analytic function $\psi(u)$ of the complex variable $u = x + iz$

$$\psi = \phi + iA/\mu_0 \ , \tag{5}$$

ϕ is the scalar potential and A the vector potential of the field (mks units). The scalar potential is chosen equal to zero on the equipotential line along Ox, as is the vector potential on the equiflux line along Oz. ψ will also be regarded as a function of the complex variable $\zeta = \xi + i\eta$.

The complex field is derived from ψ by

$$-H^* = -H_x + iH_z = \frac{d\psi}{du} = \frac{d\psi}{d\zeta}\frac{d\zeta}{du} \ . \tag{6}$$

Concerning the field behavior in the neighborhood of the vertices of the median structure cross section, such as 3 (Fig. 1), similar arguments as those developed in Ref. 2 hold. To a fine scale the tangen-

tial field along 23 varies greatly on a characteristic length of the order of the domain spacing (Fig. 3 of Ref. 2). The local component H_x at point 3 is continuous and of magnitude H_c. The averaging process of the macroscopic model entails a discontinuity, but, as discussed in Ref. 2, the overall macroscopic equilibrium is not sensitive to the value of the field on the diamagnetic side. We will also ignore complications arising in a thin perturbed sheet below the free surface, along 23 (and 2'3'), where the internal uniformity of the field is broken. Finally, in the macroscopic model, the segments 23 and 2'3' belong to symmetrical equipotential lines. In addition, the contour of the flux-free volume in the diamagnetic state, necessarily belongs to a line of constant flux

$$A_3 = A_4 = A_6 = A_\omega = A_{6'} = A_{4'} = A_{3'} = \tfrac{1}{2}A \ , \quad (7)$$

A is the total flux passing through the slab. Note that this line meets the sample surface somewhere between 3 and 6 at point 4 (Fig. 1).

As discussed in Ref. 1, the derivation of the thermodynamic potential is conducted by assuming that volumes of matter in the superconductive and normal state are initially "frozen" in a definite configuration. The intermediate state in the field penetrated region thus consists of linear laminas parallel to Oz (Fig. 3). Laminae in the superconductive state are assumed to be made of perfectly diamagnetic material. Laminas in the normal state are assumed to be made of matter with a linear and uniform magnetic susceptibility, instead of taking a zero susceptibility, as for studying penetration in the edge, in Ref. 2. The reason for this is that when domains have penetrated in the bulk of the sample, the volume in the diamagnetic state is no longer simply connected, and a macroscopic current may exist *a priori*. The magnetic moment associated with such a macroscopic current gives rise to a finite value for the magnetostatic polarization intensity J_n in normal domains. In the fictitious magnetization process which leads to the magnetic energy of the true final state, supercurrents are, at any time, proportional to the applied field so that, in the equivalent magnetostatic description, J_n is, at any time, a linear function of the fields. Thus, the normal matter can be described by a finite, constant and uniform susceptibility; uniformity is convenient but not essential since, as is well known, a great deal of arbitrariness prevails in the magnetostatic description of a given current distribution.

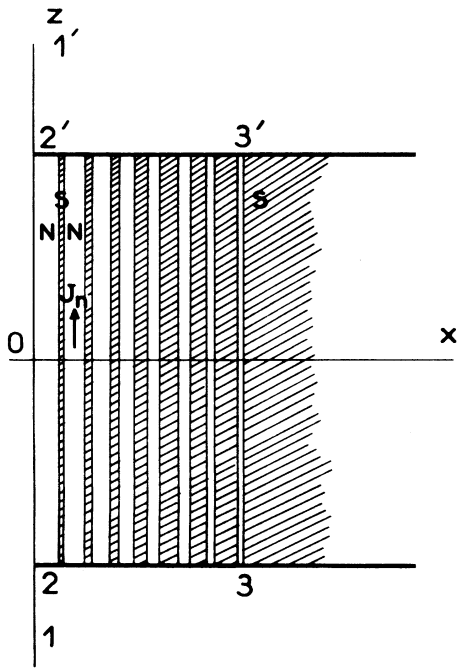

FIG. 3. Sketch of the intermediate state structure in the median region of the slab, resulting from flux penetration.

Finally, the internal structure (Fig. 3) is characterized by the uniform field H_l, such that

$$\phi_2 = \phi_3 = \tfrac{1}{2} l H_l \ , \quad (8)$$

and the following value of the induction in normal domains

$$B_n = \mu_0 (H_l + J_n) \ , \quad (9)$$

in which J_n is a linear function of the fields. The internal thermodynamic equilibrium will require B_n to be of strength $\mu_0 H_c$.

The macroscopic current $\mathcal{J}$, as derived from the circulation of the induction vector along the closed contour 33'6'63 (the internal path 33' being described in normal matter), is given by

$$\mathcal{J} = \int_{33'} J_n \, dz = J_n l \ . \quad (10)$$

The boundary conditions (7) and (8) which must be obeyed by the imaginary and real part of the potential are very simple. This leads us to introduce, as an intermediate step, the complex potential profile in the $\psi(\phi, A/\mu_0)$ plane. The possible profiles are represented Figs. 2(c) and 2(d).

The problem of determining the complex potential $\psi(\zeta)$ is now reduced to writing down the Schwarz-Christoffel formula which conformally transforms the nonhatched area of Figs. 2(c) and 2(d), bounded by the contour 12346ω6'4'3'2'1', into the upper-half ζ plane, $\eta \geq 0$ [Fig. 2(b)]. The most general potential involves a linear combination of the Figs. 2(c) and 2(d) cases, which can be written as follows:

$$\frac{d\psi}{d\zeta} = [BH_0(\zeta^2 - t^2) + C](\zeta^2 - p^2)^{-1/2}(\zeta^2 - 1)^{-1/2} \ , \quad (11)$$

where C is a constant, and the square-root determination is taken to be real and positive when ζ is real

and larger than 1. B is the dimensional parameter defined in Eq. (2).

The complex field is then deduced, with the help of Eqs. (1) and (6), as

$$-H_x + iH_z = i[H_0(\zeta^2 - t^2) + C/B] \times [(\zeta^2 - p^2)(\zeta^2 - k^2)]^{-1/2} \quad . \tag{12}$$

At large distance ($\zeta \to \infty$)

$$-H_x + iH_z = iH_0\left[1 - \frac{1}{\zeta^2}[t^2 - \tfrac{1}{2}(k^2 + p^2)]\right] + \frac{iC}{B\zeta^2} \quad , \tag{13}$$

which shows that the field reduces to the applied field $\vec{H}_0$. The $1/\zeta$ term will be used below, in the calculation of the magnetic moment.

a. Free flux distribution. The first term in the right-hand side of Eq. (11) refers to the distribution deriving from the profile 2(c). The field tends to the uniform applied field $\vec{H}_0(0, H_0)$ at large distance. The amount of flux which penetrates into the median structure is proportional to H_0. Therefore, in that distribution, flux penetrates freely and, as a result, no macroscopic current can exist; i.e., $J_n = 0$. It will be referred to as the "free flux distribution" and labeled by the subscript f. Upon integration with respect to ζ, along the real axis, the potentials $\phi_{f2} = \phi_{f3}$ and A_f are obtained as functions of the dimensions a, l, b, and the parameter t

$$\begin{aligned}\phi_{f2} = \phi_{f3} &= BH_0 \int_0^p (t^2 - \xi^2)(p^2 - \xi^2)^{1/2}(1 - \xi^2)^{-1/2}\, d\xi \\ &= BH_0(E_p - t'^2 F_p) \quad ,\end{aligned} \tag{14}$$

$$\begin{aligned}\tfrac{1}{2}A_f &= BH_0 \int_p^1 (\xi^2 - t^2)(\xi^2 - p^2)^{-1/2}(1 - \xi^2)^{-1/2}\, d\xi \\ &= \mu_0 BH_0(E_{p'} - t^2 F_{p'})\end{aligned} \tag{15}$$

($p'^2 = 1 - p^2$, $t'^2 = 1 - t^2$). Since $J_n = 0$, the induction in normal domains is simply

$$B_{fn} = 2\mu_0 \phi_{f2}/l \quad . \tag{16}$$

Moreover, denoting by n the local fraction of matter in the normal state, we have the following condition of internal consistency:

$$B_{fn} \int_0^{b/2} n\, dx = \frac{B_{fn} S_n}{2l} = \tfrac{1}{2}A_f \quad , \tag{17}$$

S_n is the total area of the slab cross section in the normal state. On account of Eqs. (14)–(16), Eq. (17) yields

$$S_n = l^2(E_{p'} - t^2 F_{p'})/(E_p - t'^2 F_p) \quad . \tag{18}$$

The parameter t is thus directly dependent on the normal area S_n. Making use of the Legendre identity[13]

$$E_p F_{p'} + E_{p'} F_p - F_p F_{p'} = \tfrac{1}{2}\pi \quad , \tag{19}$$

which entails

$$(E_p - t'^2 F_p) F_{p'} + (E_{p'} - t^2 F_{p'}) F_p = \tfrac{1}{2}\pi \quad ,$$

we can still write, from Eq. (18)

$$E_p - t'^2 F_p = \pi l^2/2(F_{p'} l^2 + F_p S_n) \quad , \tag{20}$$

$$E_{p'} - t^2 F_{p'} = \pi S_n/2(F_{p'} l^2 + F_p S_n) \quad . \tag{21}$$

b. Trapped flux distribution. The second term in the right-hand member of Eq. (11) refers to the profile of Fig. 2(d) which leads to a distribution characterized by a vanishing field at infinity and a definite amount of flux passing through the median region, proportional to the constant C. This distribution will be referred to as a "trapped flux distribution" and will be labeled by the subscript t. In a similar way, as before, the potentials are given by

$$\begin{aligned}\phi_{t2} = \phi_{t3} &= C \int_\infty^1 (\xi^2 - p^2)^{-1/2}(\xi^2 - 1)^{-1/2}\, d\xi \\ &= -CF_p \quad ,\end{aligned} \tag{22}$$

$$\begin{aligned}A_3 = A_6 = A_\omega = \tfrac{1}{2}A_t &= -\mu_0 C \int_1^p (\xi^2 - p^2)^{-1/2}(1 - \xi^2)^{-1/2}\, d\xi \\ &= \mu_0 C F_{p'} \quad ,\end{aligned} \tag{23}$$

A_t is the total trapped flux through the slab.

The induction in normal domains is given by

$$B_{tn} = \mu_0(2\phi_{t2}/l + J_n) = lA_t/S_n \quad , \tag{24}$$

whence, on substituting ϕ_{t2} and A_t from Eqs. (22) and (23), respectively,

$$J_n = 2C(F_{p'} l^2 + F_p S_n)/lS_n \quad . \tag{25}$$

A macroscopic current now exists and, from Eq. (10), is given by

$$g = 2C(F_{p'} l^2 + F_p S_n)/S_n \quad . \tag{26}$$

We now proceed to determine the constant C of the complete distribution. It will be chosen so that the flux amounts to a given value A_1. This can be achieved by the following two-stage magnetization process (Fig. 4). (i) $0 \leq H_0 \leq H_1$: flux penetrates freely in the median structure up to the value

$$A_1 = \mu_0 \pi B S_n H_1/(F_{p'} l^2 + F_p S_n) \quad . \tag{27}$$

(ii) $H_1 \leq H_0$: further increase of flux is stopped by

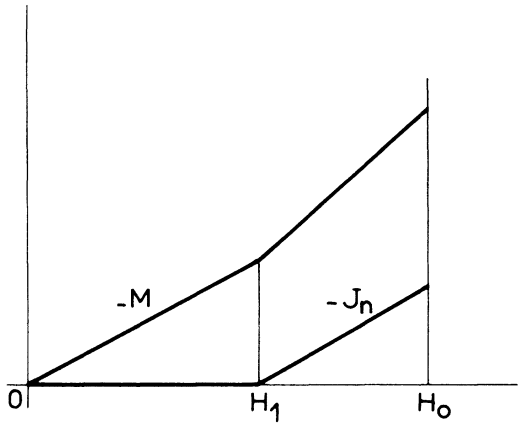

FIG. 4. Plot of the magnetic moment (M) of the slab and of the polarization intensity in normal domains (J_n), vs the applied field H_0, along the magnetization process used for the calculation of the magnetic energy, in the magnetostatic model.

superimposing a trapped flux distribution. The suited value of the constant C is readily seen to be

$$C=-\pi B(H_0-H_1)S_n/2(F_p'l^2+F_pS_n)F_p' \quad . \tag{28}$$

On account of Eqs. (11), (28), (21), and (27), the explicit expression of the complete distribution can now be written

$$\frac{d\psi}{d\zeta}=\left[BH_0\left(\zeta^2-\frac{E_p'}{F_p'}\right)+\frac{A_1}{2\mu_0F_p'}\right] \times(\zeta^2-p^2)^{-1/2}(\zeta^2-1)^{-1/2} \quad , \tag{29}$$

and the complex field as

$$-H_x+iH_z=i\left[H_0(\zeta^2-E_p'/F_p')+A_1/2\mu_0BF_p'\right] \times(\zeta^2-p^2)^{-1/2}(\zeta^2-k^2)^{-1/2} \quad . \tag{30}$$

The induction in normal domains is derived from Eqs. (17) and (24)

$$B_n=\mu_0[2(\phi_{f2}+\phi_{A2})/l+J_n]=lA/S_n \quad , \tag{31}$$

whereas the macroscopic current, still given by Eq. (26) is written, on account of Eq. (28)

$$g=-\pi B(H_0-H_1)/F_p' \quad . \tag{32}$$

It is evident from Eq. (12) that the field rises to infinity at points 3 and 6. An infinite field at 6 results from our simplifying assumption of neglecting penetration in the edges, whereas the field at 3 will be shown to drop to a finite magnitude at thermodynamic equilibrium, as is the case in Ref. 2.

III. THERMODYNAMIC POTENTIAL AND INTERNAL EQUILIBRIUM

The thermodynamic potential, already considered in Refs. 1 and 2, involves the condensation energy W_C and the magnetic energy, in the form

$$G=W_C-\mu_0\int_0^{H_0}M\,dH_0 \quad , \tag{33}$$

M is the magnetic moment of the slab, obviously parallel to Oz. The integration is carried out along the magnetization process of the previously defined frozen-in structure.

The condensation energy can be deduced from the local fraction n of matter in the normal state. Per unit volume, in units of $\frac{1}{2}\mu_0H_c^2$

$$W_C=-\frac{2}{la}\int_{\text{half cross section}}(1-n)\,dx\,dz$$

$$=-1+\frac{2}{a}\int_0^{b/2}n\,dx=-1+\frac{S_n}{la} \quad . \tag{34}$$

The simplest way of calculating the magnetic moment is based on the behavior of the polarization field at large distance,[2]

$$M=\lim_{z\to\infty}2\pi z^2[H_z(z)-H_0] \quad .$$

The behavior of $H_z(z)$, when $z\to\infty$, is given by Eq. (13). Since from Eq. (1), $\zeta\to -z/B$, we obtain for the moment per unit volume of the slab

$$I=-\frac{2\pi B^2}{la}\left[[t^2-\tfrac{1}{2}(k^2+p^2)]H_0-\frac{C}{B}\right] \quad . \tag{35}$$

In the two-stage magnetization of Fig. 4, I takes on the following values:

$$I_0=-\frac{2\pi B^2}{la}[t^2-\tfrac{1}{2}(k^2+p^2)]H_0 \quad \text{if } H_0\leq H_1 \quad , \tag{36a}$$

$$I_1=-\frac{2\pi B^2}{la}\left[[t^2-\tfrac{1}{2}(k^2+p^2)]H_0+\frac{E_p'-t^2F_p'}{F_p'}(H_0-H_1)\right] \quad \text{if } H_0\geq H_1 \quad , \tag{36b}$$

whence, for the magnetic energy in the final state under consideration, in units of $\frac{1}{2}\mu_0 H_c^2$

$$g_M = -\left(\int_0^{H_1} I_0\, dH_0 + \int_{H_1}^{H_0} I_1\, dH_1\right) \Big/ \tfrac{1}{2} la\,\mu_0 H_c^2 = \frac{2\pi B^2}{la}\left[\left[t^2 - \tfrac{1}{2}(k^2+p^2)\right]\frac{H_0^2}{H_c^2} + \frac{E_{p'} - t^2 F_{p'}}{F_{p'}}\,\frac{(H_0 - H_1)^2}{H_c^2}\right]$$

$$= \frac{2\pi B^2}{la}\left[\left(\frac{E_{p'}}{F_{p'}} - \tfrac{1}{2}(k^2+p^2)\right)\frac{H_0^2}{H_c^2} + \frac{E_{p'} - t^2 F_{p'}}{F_{p'}}\,\frac{H_1}{H_c}\,\frac{H_1 - 2H_0}{H_c}\right] .$$

On substituting $E_{p'} - t^2 F_{p'}$ from Eq. (21), H_1 from Eq. (27), and using the expression (34) of W_C, the following expression of the reduced thermodynamic potential is finally obtained

$$g(H_0, A_1, b, S_n) = -1 + \frac{S_n}{la} + \frac{2\pi B^2}{la}\left(\frac{E_{p'}}{F_{p'}} - \tfrac{1}{2}(k^2+p^2)\right)\frac{H_0^2}{H_c^2} + \frac{l A_1^2}{a\,\mu_0^2 H_c^2 S_n} + \frac{A_1^2}{la\,\mu_0^2 H_c^2}\,\frac{F_p}{F_{p'}} - \frac{2\pi B A_1 H_0}{la\,\mu_0 H_c^2 F_p} \quad . \tag{37}$$

g is thus calculated as a function of the applied field H_0, the flux A_1, the internal dimension b through the parameter p [cf. Eq. (3)], and the normal area S_n.

a. Internal equilibrium. For given values of H_0, A_1, and b, a minimum of g occurs when the normal area takes on the following value:

$$S_n = l A_1 / \mu_0 H_c \quad , \tag{38}$$

whence, from Eq. (31), the resulting value of the induction in normal domains

$$B_n = l A_1 / S_n = \mu_0 H_c \quad .$$

This is the usual requirement of internal equilibrium in the intermediate state.

We are now able to rewrite the expressions of the moment and the thermodynamic potential involving internal equilibrium. From Eqs. (36), (21), and (28), we obtain the moment in the form

$$I = -\frac{2\pi B^2}{la}\left[\left(\frac{E_{p'}}{F_{p'}} - \tfrac{1}{2}(k^2+p^2)\right)H_0 - \frac{E_{p'} - t^2 F_{p'}}{F_{p'}} H_1\right]$$

$$= -\frac{2\pi B^2}{la}\left(\frac{E_{p'}}{F_{p'}} - \tfrac{1}{2}(k^2+p^2)\right)H_0 + \frac{\pi B A_1}{la\,\mu_0 F_{p'}} \quad . \tag{39}$$

Similarly, from Eqs. (37) and (38)

$$g(H_0, A_1, b) = -1 + \frac{2\pi B^2}{la}\left(\frac{E_{p'}}{F_{p'}} - \tfrac{1}{2}(k^2+p^2)\right)\frac{H_0^2}{H_c^2} + \frac{F_p A_1 (A_1 - 2A_0)}{la\,\mu_0^2 H_c^2 F_{p'}} \quad , \tag{40}$$

where

$$A_0 = \mu_0(\pi B H_0 - F_{p'} l H_c)/F_p \tag{41}$$

would be the value of the flux if the free flux distribution were alone, in the applied field $\vec{H}_0$.

We are left with functions of the flux A_1 and the width b of the median region which allows us to analyze in detail the magnetization process, in Secs. IV and V, along the lines of our general discussion of Ref. 1.

The macroscopic current given by Eq. (32), will also be rewritten, with the present variables, as

$$g = -\pi B(H_0 - l F_{p'} H_c/\pi B - F_p A_1/\mu_0 \pi B)/F_{p'}$$

$$= F_p(A_1 - A_0)/\mu_0 F_{p'} \quad . \tag{42}$$

IV. DIAMAGNETIC AND THERMODYNAMIC PHASES

Since we have ignored the penetration in the edges, the whole sample remains in the diamagnetic state until the penetration in the center is allowed. The corresponding value of the magnetic moment during this stage can be derived from the first expression (36), with $b = 0$, $t = p = 1$, which gives, per unit volume

$$I_d = -\pi B^2 k'^2 H_0/la = -\pi k'^2 H_0/4 G_k G_{k'} \quad . \tag{43}$$

This is the law of perfect diamagnetism of the slab.

Similarly, the related value of the reduced thermodynamic potential is readily found to be

$$g_d = -1 + \pi B^2 k'^2 H_0^2/la H_c^2$$

$$= -1 + \pi k'^2 H_0^2/4 G_k G_{k'} H_c^2 \quad . \tag{44}$$

a. Thermodynamic phase. We now proceed to analyze the stability of the penetration in the median region. It has been shown in Ref. 1 that if domains could spontaneously appear in the bulk of the sample, they would do so as the potential difference between 2 and 2′ reached the value $l H_c$. The width b

would then increase with the applied field. We are going to bring out this behavior in the slab.

First of all, since the flux is assumed to penetrate the bulk of the sample freely, A_1 is an independent variable, and equilibrium occurs as $\partial g/\partial A_1 = 0$ whence $A_1 = A_0$, which means that the free flux distribution is alone, as obviously expected. The potential g reduces to

$$g_f(H_0,b) = -1 + \frac{2\pi B^2}{la}\left(\frac{E_{p'}}{F_{p'}} - \tfrac{1}{2}(k^2+p^2)\right)\frac{H_0^2}{H_c^2} - \frac{(\pi BH_0 - lF_{p'}H_c)^2}{laF_pF_{p'}H_c^2} \quad . \tag{45}$$

From Eq. (42), the macroscopic current $\mathcal{I}$ is zero, in accordance with the free penetration hypothesis.

The equilibrium value of the internal dimension b, i.e., the parameter p, is next given by minimizing g with respect to p. The derivation is carried out by making use of the derivatives of the complete elliptic functions[13]

$$\frac{dF_p}{dp} = \frac{E_p}{pp'^2} - \frac{F_p}{p}; \quad \frac{dE_p}{dp} = \frac{E_p - F_p}{p}; \quad \frac{dp'}{dp} = -\frac{p}{p'} \quad .$$

Let us first establish the result for any given A_1. Calculations are straightforward and yield

$$\frac{\partial g}{\partial p} = \frac{2\pi}{lapp'^2F_pH_c^2}\left[(E_{p'} - p^2F_{p'})BH_0 - \frac{A_1}{2\mu_0}\right]^2 \quad , \tag{46}$$

whence the equation defining the equilibrium value of b

$$G_{p'} = E_{p'} - p^2F_{p'} = A_1/2\mu_0BH_0 \quad . \tag{47}$$

In the thermodynamic phase under consideration $A_1 = A_0$. Substituting A_0 from Eq. (41)

$$G_{p'} = (\pi BH_0 - F_{p'}lH_c)/2F_pBH_0 = \pi/2F_p - F_{p'}lH_c/2F_pBH_0 \quad ,$$

and using the Legendre identity (19)

$$G_{p'}F_p = -G_pF_{p'} + \tfrac{1}{2}\pi = \tfrac{1}{2}\pi - F_{p'}lH/2BH_0 \quad ,$$

or

$$G_p = lH_c/2BH_0 = G_kH_c/H_0 \quad . \tag{48}$$

The resulting value of the thermodynamic potential is, from Eq. (45)

$$g_f(H_0) = -1 - \frac{G_kF_{p'}}{G_{k'}F_p} + \frac{\pi}{4G_kG_{k'}}\left(\frac{2G_kH_c}{H_0} + p^2 - k^2\right)\frac{H_0^2}{H_c^2} \quad . \tag{49}$$

On the other hand, Eq. (20) in which $S_n = lA_0/\mu_0H_c$, gives

$$E_p - t'^2F_p = \tfrac{1}{2}\pi\frac{l^2}{F_{p'}l^2 + F_plA_0/\mu_0H_c} = \tfrac{1}{2}\pi\frac{l^2}{F_{p'}l^2 + (l/H_c)(\pi BH_0 - F_{p'}lH_c)} = \frac{lH_c}{2BH_0} \quad , \tag{50}$$

whence, by comparing with Eq. (48)

$$t = p \quad ,$$

which means that 4 coincides with 3 (Fig. 5). The complex potential and the complex field defined by Eqs. (11) and (12) (with $C = 0$), then reduce to

$$\frac{d\psi}{d\xi} = BH_0(\zeta^2 - p^2)^{1/2}(\zeta^2 - 1)^{-1/2} \quad ; \qquad -H_x + iH_z = iH_0(\zeta^2 - p^2)^{1/2}(\zeta^2 - k^2)^{-1/2} \quad , \tag{51}$$

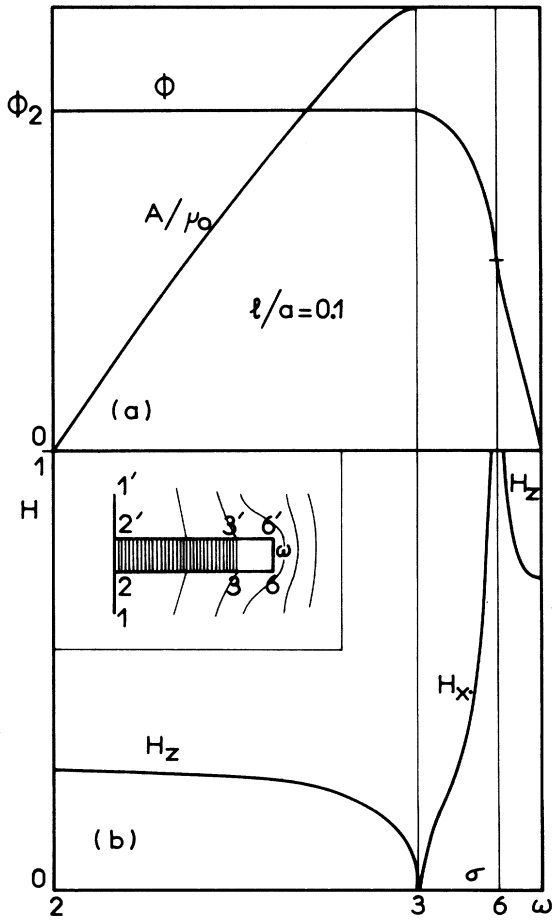

FIG. 5. Potential profiles (a) and field components (b) as functions of the abscissa σ along the contour 236ω of the slab section, in both the thermodynamic and the metastable phases. The related field configuration is represented in the inset.

which entails that the field at point 3, in the diamagnetic side, is zero. In a more detailed form, the potential and flux profiles along 23 are given by

$$\phi(\xi)+i\frac{[A(\xi)-A_3]}{\mu_0}$$
$$=BH_0(E_p-p'^2E_p)-iBH_0\left[E\left(\sin^{-1}\frac{(\xi^2-p^2)^{1/2}}{\xi p'},p'\right)\right.$$
$$\left.-p^2F\left(\sin^{-1}\frac{(\xi^2-p^2)^{1/2}}{\xi p'},p'\right)\right]. \quad (52)$$

The first term on the right-hand side is ϕ_{f2} and the second defines the flux profile represented in Fig. 5.

Thus, the tangential component of the field is continuous on passing through 3, along the surface of the slab. This result is in accordance with the continuity of the tangential component of the macroscopic field at the ends of the edge structures, previously established in Ref. 2. Let us recall that this continuity, which is a consequence of the mathematical treatment, is not in agreement with the actual macroscopic situation. This disagreement, however, can be ignored for it is ruled out by an infinitely small rearrangement of the adjacent domain structure, which has no bearing on the macroscopic equilibrium of the system.

We now turn to the determination of the thermodynamic threshold H_t. The latter is expected to be defined as the value of H_0 for which $b=0$; i.e., $t=p=1$. Since $G_1=1$, we then have, from Eq. (48)

$$H_t=lH_c/2B=G_kH_c \ , \quad (53)$$

where we have used Eq. (2).

A thermodynamic transition, indeed, could occur as $H_0=H_t$, since the thermodynamic potential g_f of the free flux phase [Eq. (49)] is just equal to g_d [Eq. (44)], as $p=1(E_{p'}=F_{p'}=\frac{1}{2}\pi, F_p=\infty)$; i.e.,

$$g_f(H_t,b=0)=g_d(H_t) \ .$$

This is the equation of the ideal transition. Furthermore, from Eqs. (14) and (49)

$$2\phi_{f2}=lH_c \ .$$

The potential difference between 2 and 2′ is lH_c, at the transition, according to the general rule given in Ref. 1.

Elimination of A_1 between Eqs. (39) and (47) yields the moment expression

$$I=-\pi B^2H_0(p^2-k^2)/la=-\pi H_0(p^2-k^2)/4G_kG_{k'} \ , \quad (54)$$

whatever the value of A_1 is. In the thermodynamic phase I takes on the value I_f obtained by substituting

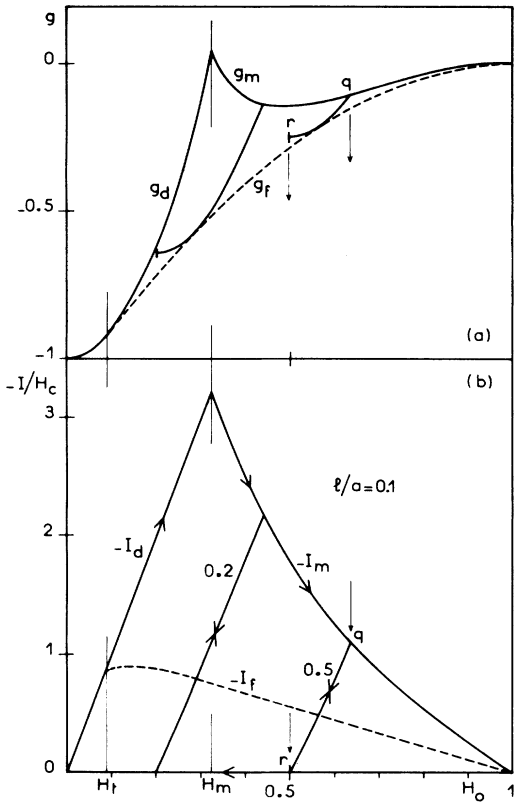

FIG. 6. (a) Plot of the reduced thermodynamic potential vs the applied field H_0 counted in units of H_c, in the diamagnetic (g_d), thermodynamic (g_f), and metastable (g_m) phases, for $l/a=0.1$. (b) Related values of the reduced magnetic moment. Also shown are the potential and moment variations along two selected "diamagnetic paths" ($A/\mu_0 aH_c=0.2$ and 0.5), obtained in decreasing field. The final part of the returning magnetization curve coincides with the axis $I=0$, in the present model. Note the strong hysteretic behavior.

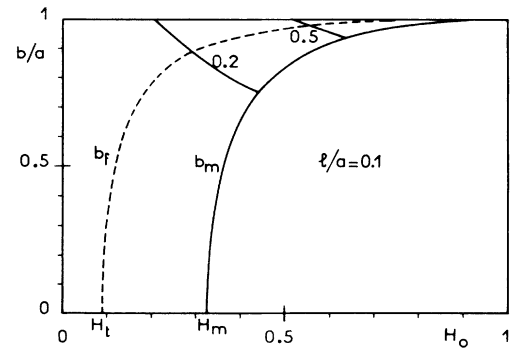

FIG. 7. Plot of the reduced width b/a of the median penetration region in the thermodynamic (b_f) and metastable (b_m) phases, vs the applied field H_0 counted in units of H_c. Transverse curves represent the variations of b/a along the selected diamagnetic paths.

p from Eq. (48).

In Fig. 6 equilibrium values of the functions g_d, g_f, I_d, and I_f are plotted versus the applied field H_0, in the case $l/a = 0.1$. Note the increase of stability in the state of free penetration, beyond the transition $H_0 = H_t$. Variations of the dimension b with the field are represented in Fig. 7. We observe a rather sharp increase, as the field has just overcome the threshold H_t, which looks like the trend of the disorder parameter in a phase transition of the second kind.

V. METASTABLE PHASE

Since a domain is prevented from appearing spontaneously by the fluxoid theorem,[1] the sample will remain in a metastable state until a value of H_0 is reached, such that domains are able to migrate from the peripheral region towards the central position 22'. This problem has been investigated for the slab, in a realistic way in Ref. 2, up to the calculation of the migration threshold as a function of dimension.

We will proceed further, in this section, by means of some simplification of the migration condition. At the starting of the migration process 7 and 7' (Fig. 1) meet at ω. $5\omega 5'$ is then a critical wall, this condition we can simplify in the present model, for a thin slab ($l \ll a$) by taking H_ω to be equal to H_c,

$$H_\omega(H_0, A_1, b) = H_c \quad . \tag{55}$$

The migration field H_m will be defined by the lowest value of H_0 for this condition to be satisfied.

Instead of what happens in the thermodynamic phase, A_1 and b are no longer independent variables, but are now related by Eq. (55). This leads, at first sight, to the state m_0 of lowest potential, on the set of $g(H_0, A_1, b)$ functions, shown in Fig. 8. This state, however, is not open to the system. Let m be the point where the locus of points connected by Eq. (55), is tangent to the external envelope of the $g(H_0, A_1, b)$ functions (Fig. 8). Assume an infinitely small displacement from m to m', requiring a small increase of the flux A_1. The system cannot remain in m' because a more stable state m'' is practicable, for the same amount of flux. The transition $m'm''$ only needs a small rearrangement of the intermediate state structure, in which b is varied from some value $b_{m'}$ to another one $b_{m''}$. But in the state m'', the migration condition is no longer fulfilled ($H_\omega < H_c$), so that the system cannot proceed further towards m_0.

It follows that the system gets hung up close to the state m, which is defined both by Eq. (55) and

$$\partial g(H_0, A_1, b)/\partial b = 0 \quad . \tag{56}$$

The set of states $m(H_0)$, which will be referred to as belonging to a metastable phase, completely determine the migration stage in an increasing field, as emphasized in Ref. 1.

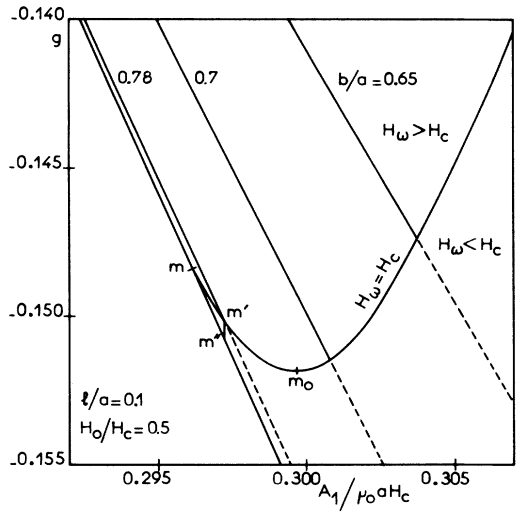

FIG. 8. Set of curves showing the dependence of the thermodynamic potential $g(H_0, A_1, b)$ on the flux A_1 and the dimension b, for a fixed value $H_0 = \frac{1}{2}H_c$ of the applied field. The g curves are represented by small arcs of parabola (close to straight-line segments in the range of interest), labeled with the selected values of b/a. Also shown is the locus of the points obeying the migration condition ($H_\omega = H_c$).

The metastable equilibrium value of b is defined by Eq. (56). The calculation of the partial derivative, early performed, yields Eq. (47).

Let us now examine the potentials and fields in the metastable phase. Taking Eq. (47) into account, Eqs. (29) and (30) give formally the same as Eq. (51). The parameter p, however, is no longer defined by Eq. (48). From Eq. (51), for $\zeta = 0$

$$H_\omega = H_0 p/k \quad ,$$

which leads to the following expression of the simplified migration condition (55)

$$p = kH_c/H_0 \quad . \tag{57}$$

The dimension b is deduced with the help of Eq. (4). Variations of b as a function of H_0 are shown in Fig. 7 in the case $l/a = 0.1$.

Equations (47) and (57) both determine the parameters A_1 and p, at any value of H_0, along the migration process. The threshold H_m is obviously defined by the additional condition $b = 0$, or $p = 1$, which yields

$$H_m = kH_c \quad . \tag{58}$$

The same is obtained if we impose $H_\omega = H_c$ in the diamagnetic phase, which is not at all surprising.

The expression (40), in which we take into account Eqs. (47) and (57), defines the potential g_m of the

metastable phase in the true state

$$g_m(H_0) = -1 + \frac{\pi(p^2-k^2) - 4G_pG_{p'}}{4G_kG_{k'}} \frac{H_0^2}{H_c^2} + \frac{2G_{p'}}{G_{k'}} \frac{H_0}{H_c} \quad . \tag{59}$$

H_m is the true transition field, instead of the ideal H_t, and corresponds to a thermodynamic equilibrium, in the usual sense, between the diamagnetic and the metastable phases; i.e.,

$$g_m(H_m, b=0) = g_d(H_m)$$

as it can be easily verified with Eqs. (44) and (59).

The expression (54) of the moment still remains. On inserting p from Eq. (57), we obtain the value I_m pertaining to the metastable phase.

As H_0 approaches H_c, the median region in the intermediate state spreads over the whole volume and finally, the sample transits into the normal state. We have, indeed, in Eq. (59), when $H_0 = H_c$, $p = k$

$$g_m(H_c) = 0 \quad .$$

g_m is plotted in Fig. 6 versus the applied field H_0, in the typical case $l/a = 0.1$ [Fig. 6(a)], along with the moment I_m [Fig. 6(b)]. $g_m(H_0/H_c)$ is seen to be higher than the ideal value g_f in the whole range. This is why we have regarded the states obtained in the migration stage as metastable ones. Note that, because of the irreversibility of the migration mechanism, g_m can take on positive values and the magnetic moment, beyond H_m, is no longer derived from the slope of the $g(H_0)$ law. Also it is worth while to note the strong departure of the moment function $-I_m(H_0)$ from the ideal one, as experimentally observed.[10-12]

a. Field distribution and macroscopic current. Because the field distribution is formally given by Eqs. (51), the trend of the fields, in the metastable phase, is still represented by Fig. 5. Thus the thermodynamic and metastable phases are quite similar for the field distribution, but differ by the amount of penetrated flux and by the equilibrium value of the internal dimension b (Fig. 7).

The main consequence of the flux A_1 to be different from A_0 is the occurrence of a macroscopic current $\mathcal{J}$ in the metastable phase. This current is given by Eq. (42) in which A_1 and p are substituted from Eqs. (47) and (57).

b. Diamagnetic paths in decreasing field and hysteretic behavior. Assuming that the system has reached some state q in the migration stage [Fig. 6(b)], let us lower the field from H_q. This decrease entails a reduction of H_ω below H_c and, as a result, domains cannot enter the slab. But they do not escape from the inside either, as long as the metastable equilibrium value of b is smaller than a. Therefore, the magnetization is governed by a constant value of the flux, equal to the initial one

$$A_q = 2\mu_0 B H_q G_{p_q'} = \mu_0 a H_q G_{p_q'}/G_{k'} \quad ,$$

where $p_q = kH_c/H_q$. The related values of the moment I are still given by Eq. (53), in which p is a function of $H_0 < H_q$ defined by

$$A_q = \mu_0 a H_0 G_{p'}/G_{k'} \quad .$$

Examples of constant flux paths for two selected values of the flux, $A/\mu_0 a H_c = 0.2$ and 0.5, are shown in Fig. 6. The moment curves [Fig. 6(b)] are nearly parallel to the initial diamagnetic law whence the name of "diamagnetic path" currently used.[14,15] They cross the ideal curve I_f at a point where the related thermodynamic potential curve tangents the ideal one [Fig. 6(a)]. The system, however, remains in a metastable state even below the crossing point. Domains indeed are not able to leave the slab in that range either, because of $H_\omega < H_c$ or, in a more realistic way, 7 and 7′ are distinct from ω (Fig. 1). It follows that the flux remains equal to A_q until the state r, in which $b = a$, or $p = k$, is reached. In this state $H_0 = H_r = A_q/\mu_0 a$ and $I = 0$. From this point onwards, if the field is decreased further, the returning magnetization curve is the axis $I = 0$. In fact, the same result is obtained whatever the q starting point is.

Experimentally, diamagnetic paths, such as qr, are currently observed, but the return magnetization curve does not coincide with the axis $I = 0$. This disagreement is a consequence of the simplifying assumptions of the present model. Before reaching the state r, the moment is critically dependent on the possibility that the domains can be expelled out of the sample which, in turn, depends on the detailed configuration of the penetration in the edge. The question must therefore be revised in a more realistic treatment.

In summary, it can be ascertained that most of the magnetization law of the slab is contributed by the metastable mechanism which is responsible for a great deal of hysteresis.

VI. CONCLUSION

A complete illustration of the thermodynamics of the magnetization of a type-I superconductor has been worked out in the geometry of an infinite flat slab, of rectangular cross section, in a perpendicular magnetic field.

The metastable character of the magnetization process, previously discussed in a general way, has been

emphasized by a detailed analytic calculation of the suitable thermodynamic potential, which permits the analysis of the migration mechanism, the occurrence of a macroscopic current, and of the hysteretic behavior. Comparison is made with the underlying, but unattainable, thermodynamic process.

More precise calculations, taking into account penetration in the edges, should be possible, by means of a more elaborated analytic solution of the relevant Dirichlet's problem. Our model, however, brings out the physics of the magnetization in a quite simple mathematical scheme.

---

*Associé au CNRS No. 251.

[1]A. Fortini and E. Paumier, Phys. Rev. B 14, 55 (1976).
[2]A. Fortini, A. Hairie, and J-P. Girard, J. Math. Phys. 20, 2139 (1979).
[3]W. de Sorbo and W. A. Healy, Cryogenics 4, 257 (1964).
[4]F. Haenssler and L. Rinderer, Helv. Phys. Acta 40, 659 (1967).
[5]H. Träuble and U. Essmann, Phys. Status Solidi 18, 813 (1966).
[6]P. R. Solomon, Phys. Rev. 179, 475 (1969).
[7]R. Olafsson and J. F. Allen, J. Phys. F 2, 123 (1972).
[8]H. Kirchner and A. Kiendl, Phys. Lett. A 39, 293 (1972).
[9]D. C. Baird and L. S. Wright, J. Low Temp. Phys. 8, 177 (1972).
[10]J. Provost, E. Paumier, and A. Fortini, J. Phys. F 4, 439 (1974).
[11]H-U. Habermeier, Phys. Status Solidi A 39, 203 (1977).
[12]U. Essmann, W. Wiethaup, and H-U. Habermeier, Phys. Status Solidi A 43, 151 (1977).
[13]I. S. Gradshteyn and I. M. Ryzhik, *Tables of Integrals, Series, and Products,* translated by Alan Jeffrey (Academic, New York, 1965).
[14]D. G. Schweitzer and B. Bertman, Phys. Rev. 152, 293 (1966).
[15]J-P. Girard, E. Paumier, and A. Fortini, J. Phys. (Paris) 32, 895 (1971).